 CMES, vol.48, no.3, pp.241-268, 2009

Fast Identification of Poroelastic Parameters from Indentation Tests

M. Galli and M.L. Oyen[1]

Abstract: A novel approach is presented for the identification of constitutive parameters of linear poroelastic materials from indentation tests. Load-controlled spherical indentation with a ramp-hold creep profile is considered. The identification approach is based on the normalization of the time-displacement indentation response, in analogy to the well-known one-dimensional consolidation problem. The identification algorithm consists of two nested optimization routines, one in the time-displacement domain and the other in a normalized domain. The procedure is validated by identifying poroelastic parameters from the displacement-time outputs of finite element simulations; the new identification scheme proves both quantitatively reliable and fast. The procedure is also tested on the identification of the constitutive parameters of gelatin gel and bone from experimental indentation data and succeeds in providing quantitative results almost in real time.

Keywords: Indentation, Poroelasticity, Identification, Master Curves, Permeability.

1 Introduction

Indentation is a common technique for testing the mechanical behavior of almost any material at length scales ranging from nanometers, for nanoindentation, to millimeters in the case of traditional indentation. Due to the potential for measurement and mapping of local properties (Cuy et al., 2002), and associated with minimal specimen preparation requirements, indentation techniques are particularly suitable for the testing of biological materials (Ebenstein and Pruitt, 2006). The cost of the simplicity of the actual test execution is that the extraction of the values of the constitutive parameters from the test output (typically load-displacement, load-time or displacement-time curves) is not always straightforward, often requiring inverse analysis.

[1] Cambridge University Engineering Dept.,Trumpington St., Cambridge, CB2 1PZ, UK

Finite element (FE) modeling is a powerful and versatile means which allows for extraction of much information from indentation results, for example the elasto-plastic stress-strain curve of a metal (Bucaille et al., 2003), the matrix flow-stress in a composite (Bucaille et al, 2004), and the poroelastic, viscoelastic or poroviscoelastic parameters of a hydrogel (Galli et al., 2009; Liu et al., 2008; Olberding and Suh, 2006). Nevertheless inverse FE modeling is computationally too expensive to be employed when large amounts of data need be analyzed, as it is typically the case of grid indentation mapping (Constantinides et al., 2008) where up to thousands of indentation tests are carried out. Property mapping of biological tissues by indentation is particularly attractive not only to investigate the material structure and properties but also for diagnostic purposes – spherical indentation can be seen as nothing but a sophisticated version of palpation as used by physicians for diagnosis. In massive property mapping experiments, identification methods faster than FE must be employed. Possible approaches include the use of methods based on a database of solutions: grids of dimensional solutions (Gupta et al., 2008), neural networks (Huber and Tsakamakis, 1998; Huber et al., 2001; Liu et al., 2009) and master curves (Hsueh and Miranda, 2003). Compared to other techniques the master-curve methods, being based on a normalized material response, have the intrinsic advantage that their applicability is not limited to the range of material properties considered for the construction of the database itself.

In the case of biological materials the constitutive behavior can often be assumed to be linear poroelastic (e.g. bone (Cowin, 2004), soft tissues (Simon, 1992), gels (Hui et al., 2005) and reinforced gels (Gupta et al., 2008)). The idea of obtaining master curves for the spherical indentation of a linear poroelastic half-space was first proposed by Agbezuge and Deresiewicz (1974) and further developed by Deresiewicz (1976), who considered step-loading conditions. In both cases the problem is solved using an analytical method which, however, requires a numerical solution, based on the displacement functions by McNamee and Gibson (1960) and Laplace-Hankel double transform, following an approach often used in similar problems as shown by Selvadurai (1994, 2007). Nevertheless the applicability of this pioneering approach to actual experimental data is limited by the hypothesis of step-loading conditions, which are virtually impossible to obtain experimentally even for small permeability values (Galli and Oyen, 2008). The idea of using master-curves for the identification of poroelastic parameters was more recently revisited by Hui and Muralidharan (2005), who considered the two dimensional problem of an infinitely long rigid circular cylinder indenting on a poroelastic half-space. Also in this case step-loading conditions are assumed, moreover the considered geometry is not representative of three dimensional experimental conditions.

In the present work to the master curve approach for spherical indentation is re-

viewed and extended to ramp-hold test profiles. Its theoretical basis are presented by showing the parallel with ramp-hold one-dimensional consolidation, a problem which can be solved analytically. The indentation master curves are obtained by FE modeling. An algorithm for the fast identification of constitutive parameters using a master curve database is proposed and validated by identifying constitutive parameters from the results of FE simulations of indentation tests on linear poroelastic materials with incompressible constituents. Finally two examples of the application of the method on actual experimental data, from a gelatin gel and from bone, are presented.

2 Linear Isotropic Poroelasticity Theory

This work considers the quasi-static indentation testing of a saturated linear isotropic poroelastic medium, that is a porous isotropic solid skeleton saturated with a pore fluid. Therefore it is useful to summarize the equations which govern the mechanical behavior of such a material. The formalism and definitions adopted herein conform to those used by Detournay and Cheng (1993), which is one of the standard references in the field together with the monographs by Wang (2000) and Coussy (2004), to which the reader is referred for a more extensive introduction to the theory.

The constitutive equation for the solid skeleton is

$$\sigma_{ij} + \alpha p \delta_{ij} = 2G\varepsilon_{ij} + \frac{2G\nu}{1-2\nu}\varepsilon_{kk}\delta_{ij}, \tag{1}$$

where σ_{ij} and p are the stress tensor and pore pressure, respectively; ε_{ij} the strain tensor, G the shear modulus, ν the drained Poisson's ratio and δ_{ij} Kronecker's tensor. Note that G and ν are the elastic properties of the porous medium seen as a homogeneous linear elastic material and not those of the solid phase itself. The constitutive parameter α is the variation of the fluid volume in a material unit volume due to the volumetric change, when the pore pressure can return to its initial state. The range of variation of α is $[0,1]$. The response of the fluid phase is expressed by

$$p = \frac{2G(\nu_u - \nu)}{\alpha^2(1-2\nu_u)(1-2\nu)}(\zeta - \alpha\varepsilon_{kk}), \tag{2}$$

with ν_u being the undrained Poisson's ratio and ζ the variation of fluid volume per unit volume of porous material. Fluid motion is described by means of Darcy's law:

$$q_i = -\kappa p_{,i}, \tag{3}$$

where q_i is the specific discharge vector, defined as the rate of fluid volume which crosses a unit area of porous solid having the normal in the x_i direction and κ the permeability coefficient defined as the ratio between the intrinsic permeability and the fluid (dynamic) viscosity. Note that in (3) body forces (and the effect of gravity) are assumed to be negligible. Therefore they are not present in the equilibrium equation, as well:

$$\sigma_{ij,j} = 0. \tag{4}$$

Finally the local continuity equation for the fluid mass completes the problem:

$$\frac{\partial \zeta}{\partial t} + q_{i,i} = 0, \tag{5}$$

where it is assumed that there is no fluid source (the right-hand side set to zero). Equations (1–5) show that five parameters are required to fully characterize a saturated linear isotropic poroelastic medium: four elastic constants and the permeability, κ. Several different sets of elastic parameters can be chosen, and the choice typically depends on the problem to be tackled. In the present case the following set is considered: G, ν, α, ν_u.

3 One-dimensional Consolidation with Ramp-Hold Load Profile

One-dimensional consolidation is a classical problem in soil mechanics – probably *the* classical problem, as it was first studied by Terzaghi (1923). In a uniaxial consolidation test (also called an oedometer test), load is applied under drained conditions on the surface of a saturated poroelastic layer of a given initial thickness L, which lies on an impermeable rigid substrate as shown in the schematic in figure 1 a). While the classical approach assumes step-loading, in the present case a ramp-hold load profile is considered. The solution to this problem is reported herein because the problem itself presents analogies with indentation, and the way its solution can be normalized inspired the master curve approach developed for indentation. Moreover, to the authors' knowledge, the analytical solution for one-dimensional consolidation with a ramp-hold profile is reported in the literature either in part, e.g. only in terms of pore pressure, or using a different normalization (Schiffman, 1958; Olson, 1977; Wang, 2000).

In the case of uniaxial strain ε_{xx}, from now on indicated by ε for simplicity, the constitutive equation (1) for stress component σ_{xx} (replaced with σ) reduces to

$$\sigma = \frac{2G(1-\nu)}{1-2\nu}\varepsilon - \alpha p. \tag{6}$$

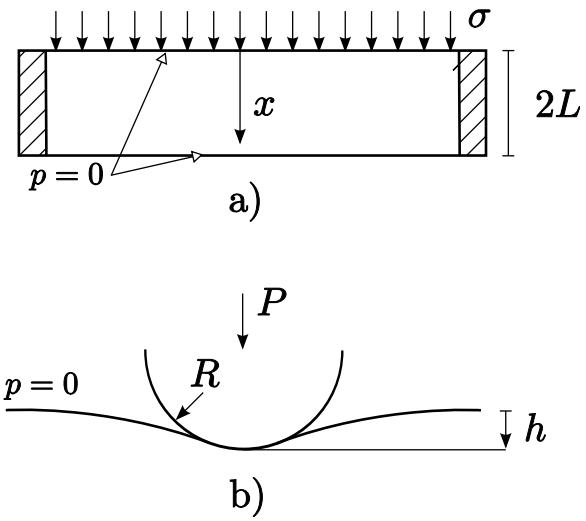

Figure 1: Schematics of a) one-dimensional consolidation and b) spherical indentation of a half-space.

By combining (2) with (3) and (5) and expressing ε using (6) the diffusion equation for the pore pressure is obtained:

$$\frac{\partial p}{\partial t} - c\frac{\partial^2 p}{\partial x^2} = -\frac{\nu_u - \nu}{\alpha(1-2\nu)(1-\nu_u)}\frac{d\sigma}{dt}, \tag{7}$$

where c is the diffusivity coefficient:

$$c = \frac{2\kappa G(1-\nu)(\nu_u - \nu)}{\alpha^2(1-2\nu)^2(1-\nu_u)}. \tag{8}$$

In the case of ramp-hold load profile with rise time t_R and constant load rate $\gamma = -d\sigma/dt$ two diffusion equations have to be solved:

$$\frac{\partial p}{\partial t} - c\frac{\partial^2 p}{\partial x^2} = \gamma\frac{\nu_u - \nu}{\alpha(1-2\nu)(1-\nu_u)},\ 0 \le t < t_R, \tag{9}$$

$$\frac{\partial p}{\partial t} - c\frac{\partial^2 p}{\partial x^2} = 0,\ t \ge t_R. \tag{10}$$

The boundary conditions are

$$p(0,t) = 0, \tag{11}$$

$$p(2L,t) = 0, \tag{12}$$

while the initial condition (for $t = 0$) is

$$p(x,0) = 0, \tag{13}$$

and the condition for $t = t_R$ is:

$$p_r(x,t_R) = p_h(x,t_R), \tag{14}$$

where p_r and p_h are the pressure functions obtained from (9) and (10), respectively. Equation (9) is a diffusion equation with constant right hand side. Its solution (Kochina, 1971) is

$$p(x,t) = \gamma \frac{\nu_u - \nu}{\alpha(1-2\nu)(1-\nu_u)} \sum_{n=1,3,\ldots}^{\infty} \frac{16L^2}{n^3\pi^3 c} \left[1 - \exp\left(-\frac{n^2\pi^2 c}{4L^2}t\right)\right] \sin\frac{n\pi x}{2L}. \tag{15}$$

Note that this expression is equivalent to that reported by Wang (2000) for the pressure of a finite poroelastic layer subjected to uniformly increasing load, with the difference that herein also the time-independent terms in the expression are included in the Fourier expansion. The diffusion equation for the hold segment (10) is homogeneous and yields the following expression for the pressure field:

$$\begin{aligned} p(x,t) = \sum_{n=1,3,\ldots}^{\infty} \gamma \frac{\nu_u - \nu}{\alpha(1-2\nu)(1-\nu_u)} \frac{16L^2}{n^3\pi^3 c} \left[\exp\left(-\frac{n^2\pi^2 c}{4L^2}(t-t_R)\right)\right. \\ \left. - \exp\left(-\frac{n^2\pi^2 c}{4L^2}t\right)\right] \sin\frac{n\pi x}{2L}. \end{aligned} \tag{16}$$

To find the expressions for the displacement $u(x,t)$, it is sufficient to introduce (15) and (16) in (6) and integrate the obtained strain $\varepsilon = \partial u/\partial x$ imposing the boundary condition $u(2L,t) = 0$. The displacement $u(x,t)$ during the ramp is given by

$$\begin{aligned} u(x,t) = \frac{\gamma(1-2\nu)}{2G(1-\nu)} \left\{ t(2L-x) - \frac{\nu_u - \nu}{(1-2\nu)(1-\nu_u)} \sum_{n=1,3,\ldots}^{\infty} \frac{32L^3}{n^4\pi^4 c} \right. \\ \left. \times \left[1 - \exp\left(-\frac{n^2\pi^2 c}{4L^2}t\right)\right] \left(\cos\frac{n\pi x}{2L} + 1\right) \right\}, \end{aligned} \tag{17}$$

while that for the hold segment by:

$$\begin{aligned} u(x,t) = \frac{\gamma(1-2\nu)}{2G(1-\nu)} \left\{ t_R(2L-x) - \frac{\nu_u - \nu}{(1-2\nu)(1-\nu_u)} \sum_{n=1,3,\ldots}^{\infty} \frac{32L^3}{n^4\pi^4 c} \right. \\ \left. \times \left[\exp\left(-\frac{n^2\pi^2 c}{4L^2}(t-t_R)\right) - \exp\left(-\frac{n^2\pi^2 c}{4L^2}t\right)\right] \left(\cos\frac{n\pi x}{2L} + 1\right) \right\}. \end{aligned} \tag{18}$$

The solution of the problem, as it is the case for step-loading conditions (Detournay and Cheng, 1993), can be rewritten in terms of non-dimensional time

$$\tau = \sqrt{\frac{ct}{4L^2}} \tag{19}$$

and non-dimensional surface displacement (often called 'degree of consolidation')

$$u^* = \frac{u(0,t) - u_0(0,t)}{u_\infty(0,t) - u_0(0,t)}, \tag{20}$$

where

$$\begin{aligned} u_0(0,t) &= \frac{\gamma t L(1-2\nu_u)}{G(1-\nu_u)},\ 0 \le t < t_R, \\ u_0(0,t) &= \frac{\gamma t_R L(1-2\nu_u)}{G(1-\nu_u)},\ t \ge t_R, \end{aligned} \tag{21}$$

and

$$\begin{aligned} u_\infty(0,t) &= \frac{\gamma t L(1-2\nu)}{G(1-\nu)},\ 0 \le t < t_R, \\ u_\infty(0,t) &= \frac{\gamma t_R L(1-2\nu)}{G(1-\nu)},\ t \ge t_R. \end{aligned} \tag{22}$$

Note that u^* can vary in the interval $[0,1)$. From expressions (21) and (22) the physical meaning of $u_0(0,t)$ and $u_\infty(0,t)$ can be inferred: $u_0(0,t)$ is the surface displacement which would occur if the actual load at instant t were applied in step-loading conditions (under undrained conditions) on the virgin material, while $u_\infty(0,t)$ is the corresponding settlement for $t \to \infty$ when the pore pressure field vanishes. Note that $u_0(0,t)$ and $u_\infty(0,t)$ correspond to the elastic solutions to the problem when Poisson's ratio is ν_u and ν respectively. By introducing (17), (18), (21) and (22) in (20) the expression relating the non-dimensional surface displacement to the non-dimensional time τ is obtained:

$$u^*(\tau) = 1 - \sum_{n=1,3,\ldots}^{\infty} \frac{8}{n^4\pi^4\tau^2}\left(1 - \exp\left(-n^2\pi^2\tau^2\right)\right) \qquad 0 \le \tau \le \tau_R \tag{23}$$

$$u^*(\tau) = 1 - \sum_{n=1,3,\ldots}^{\infty} \frac{8}{n^4\pi^4\tau_R^2}\left[\exp\left(-n^2\pi^2\left(\tau^2 - \tau_R^2\right)\right) - \exp\left(-n^2\pi^2\tau^2\right)\right] \qquad \tau \ge \tau_R, \tag{24}$$

where $\tau_R = \sqrt{ct_R/4L^2}$.

The obtained expressions for $u^*(\tau)$ represent a master curve, in the sense that, given τ_R, it is unique for all the materials and specimen geometries. Plots of master curves corresponding to different values of τ_R are reported in figure 2. There is one master curve for the ramp, from which the master curves for the hold segment depart with the abscissa of the transition kink point being τ_R. All the master curves lie between the two limit cases of an indefinitely long ramp ($\tau_R \to \infty$) and of step-loading conditions ($\tau_R = 0$), which is the classical oedometric master curve (Detournay and Cheng, 1993):

$$u^*(\tau) = 1 - \sum_{n=1,3,\ldots}^{\infty} \frac{8}{n^2\pi^2}\left(1 - \exp\left(-n^2\pi^2\tau^2\right)\right). \tag{25}$$

It is important to highlight that the one-dimensional consolidation test, in which the surface displacement-time profile is recorded, allows for the determination of 3 of the 5 poroelastic constitutive parameters in whichever domain, ut or $u^*\tau$, the fit of experimental data is carried out. In the displacement-time functions (17) and (18) three ratios containing the constitutive parameters can be isolated: $(1-2\nu)/[2G((1-\nu)]$, $(\nu_u-\nu)/[(1-2\nu)(1-\nu_u)]$ and c, defined by (8), while in the normalized domain G, ν and ν_u, appear in the normalization of displacement (20) and c in the normalization of time (19). Note that the permeability κ and the parameter α only appear in the diffusivity coefficient c therefore, if both are to be determined, even when the other three constitutive parameters are known only the ratio κ/α^2 can be identified.

4 Spherical Indentation with Ramp-Hold Load Profile

The normalization of time and displacement in the case of spherical indentation of a poroelastic half-space, figure 1 b), is analogous to that for one-dimensional consolidation. The non-dimensional time t^* is given by (Agbezuge and Deresiewicz, 1974)

$$t^* = \sqrt{\frac{ct}{Rh(t)}}, \tag{26}$$

where R is the indenter radius and $h(t)$ the indentation depth. Note that for one-dimensional consolidation, definition (19), the denominator is the layer thickness $2L$ which has the physical meaning of being twice the length of the 'drainage path' (the longest distance the fluid has to cover to escape the medium) while in (26) it is the contact radius $\sqrt{Rh(t)}$, for which the same meaning cannot be assumed. The non-dimensional indentation depth is

$$h^* = \frac{h(t) - h_0(t)}{h_\infty(t) - h_0(t)}, \tag{27}$$

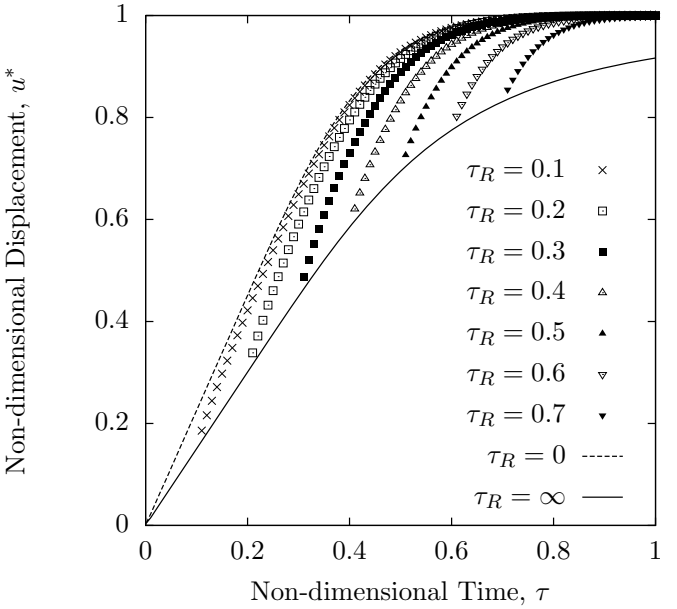

Figure 2: Master curves for one-dimensional consolidation with a ramp-hold profile: the hold segment master curves for the different non-dimensional rise times τ_R, plotted with points, lie between the ramp (solid line) and step-loading (dashed line) master curves.

where, analogously to one-dimensional consolidation, $h_0(t)$ is the indentation depth which would be measured if the actual load at instant t were applied in step-loading conditions (under undrained conditions) on the virgin material and $h_\infty(t)$ is the corresponding indentation depth at $t = \infty$ when the pore pressure field vanishes. These two limiting situations again correspond to the elastic solutions when Poisson's ratio is ν_u and ν.

As stated previously no closed-form analytical solution for the poroelastic indentation problem is available, therefore FE modeling was utilized. A master curve library was built imposing that the constituents are incompressible ($\alpha = 1$ and $\nu_u = 0.5$). This assumption is characterized by the strongest poroelastic effect, therefore the obtained master curves are more reliable, and in particular the normalization of displacement (27) since the difference $h_\infty(t) - h_0(t)$ is larger. Note that both the extension of the contact area and the contact pressure distribution depend on Poisson's ratio, therefore each pair (ν_u, ν) leads to a different set of master curves (Deresiewicz, 1976). In the present work the attention was limited to the case $\nu_u = 0.5$, which is a very common assumption in soil mechanics, for gels

(Chiarelli, 2004; Lin and Hu, 2006) and, in first approximation, for soft tissues (Simon, 1992).

An axisymmetric FE model of the indentation process was developed using ABAQUS (Version 6.7, SIMULIA, Providence, RI, USA). The model is sufficiently large for the specimen to be considered a half-space (the maximum obtained indentation depth was approximately $1/1000$ of the thickness of modeled poroelastic layer). The indenter was modeled as an analytical rigid surface and the contact between the indenter and the poroelastic half-space surface was imposed to be frictionless. The poroelastic material was assumed to be saturated. The half-space was discretized using eight-node elements with biquadratic displacement interpolation, bilinear pore pressure interpolation, and reduced integration. It was assumed that water can diffuse freely across the entire surface of the half-space, including the contact region (the indenter is permeable). Given the purpose of the present work, which is aimed at presenting the identification methodology, only the case of a permeable indenter was considered, however the approach can also be applied to the case of an impermeable indenter (e.g. by adopting the modeling strategy proposed by Warner et al. (2001)). Since an accurate estimation of the values of h_0 and h_∞ is crucial for obtaining reliable $h^*(t^*)$ master curves, FE modeling was used to compute the elastic limits (i.e. for ν_u and ν) rather than using either Hertz's formula (Johnson, 2003) or its 'corrected' version by Hay and Wolff (2001). For the elastic model, eight-node elements with biquadratic displacement interpolation, reduced integration, hybrid with linear pressure interpolation were employed (the hybrid formulation is to be preferred in the case of material incompressibility, as is the case of the simulations to assess the values of $h_0(t)$). The master curve database was built by parameterizing the FE model: ν varied in the range $[0-0.45]$ with a 0.01 step and for each of these values 17 different rise times (loading rates) were considered (the imposed load was kept constant). Therefore approximately 800 simulations were required.

The master curves were built using only the results corresponding to the hold segment and, in particular, the master curve for the ramp was built using $h(t_R)$ values from simulations with different rise times. This strategy was chosen because results corresponding to the ramp, and especially to its initial stages, can present oscillations which are due the fact that in the FE model the contact radius varies discretely, therefore an increase in load does not necessarily lead to an increase in contact radius (Mesarovic and Fleck, 1999). Although this does not affect the overall smoothness of the solution for the $h(t)$ domain it leads to a non-negligible noise when the $h^*(t^*)$ values are computed, because the normalization (27) is carried out by computing h_0 and h_∞ values from the value of the corresponding applied load.

The master curves for the extreme values of Poisson's ratio, 0 and 0.45, and dif-

ferent rise times are reported in figure 3. The curves are plotted for the non-dimensional time interval $0.2 \leq t^* \leq 4$ because for $t^* > 4$ they are nearly horizontal (therefore not suitable for identification) while $t^* \approx 0.2$ corresponds to the shortest rise time which was considered. Smaller values of the inferior limit of the interval could be obtained by adopting shorter rise times (and for $t_R = 0$ the solution by Deresiewicz (1976)), however this would not lead to a significant improvement of the parameter identification results because, as a general rule, the experimental data corresponding to the initial stages of the test are de-weighted because of the uncertainties related to the onset of contact. By comparing the curves corresponding to $\nu = 0$ and $\nu = 0.45$ it can be noted how the consolidation process advances faster when Poisson's ratio is larger, as could be expected, since the total time-dependent displacement is proportional to the difference between ν_u and ν: for step-loading conditions and using Hertz's formula (Selvadurai, 2004), the ratio of h_∞ to h_0 is given by

$$\frac{h_\infty}{h_0} = \left(\frac{1-\nu}{1-\nu_u} \right)^{\frac{2}{3}}. \tag{28}$$

This implies that the identification of material parameters is more delicate when the difference between the values of the undrained and drained Poisson's ratios is small, because the time-dependent displacement to be experimentally measured is small.

When comparing one-dimensional consolidation master curves (figure 2) with those for indentation (figure 3), the analogy between the two problems stands out: the portions of master curve corresponding to hold segments depart from that for the ramp with a marked increase in the slope (kink point) and the master curves corresponding to infinite rise time and to step-loading (not plotted for the indentation) are lower and upper bounds, respectively, which define the region where normalized experimental points can lie.

5 Identification Algorithm

The key component of an identification method is the optimization algorithm which has to be reliable and sufficiently efficient in terms of required computing time, especially when dealing with large amounts of data. The procedure presented herein is based on MATLAB® Optimization Toolbox™(Version 7.4, The MathWorks, Natick, MA, USA) and in particular on its non-linear least-squares optimization routine, the use of which in the context of material property identification is reported in the literature (Cugnoni et al., 2007; Galli et al., 2008).

Given the datapoints $(u_1, y_1), \ldots, (u_m, y_m)$ of the curve to be fit and the fitting model $M(\boldsymbol{x}, u)$ (governed by a set of parameters $\boldsymbol{x}$), the goal of the identification procedure

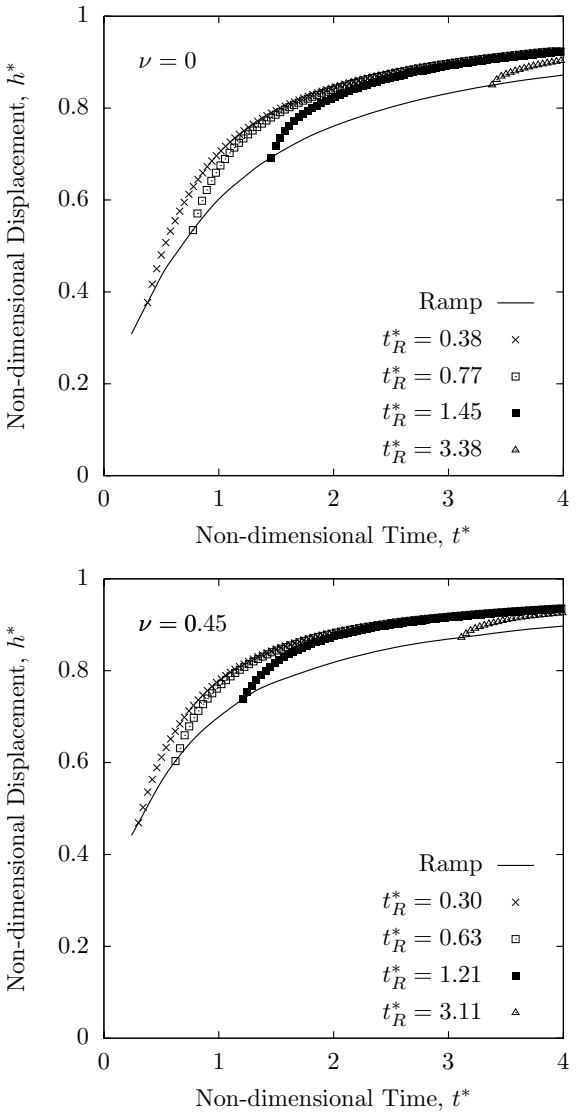

Figure 3: Master curves for spherical indentation with a ramp-hold profile for $\nu = 0$ (top) and $\nu = 0.45$ (bottom) and different rise times (of increasing values from left to right). Consolidation advances faster when Poisson's ratio is higher because the total time dependent displacement is smaller, as shown in equation (28). The master curves for spherical indentation are analogous to those for one-dimensional consolidation (figure 2) with the different curves for the hold segment departing from that of the ramp.

is to find the set of parameters $\boldsymbol{x}^{id}$ which provides the best fit. For any choice of $\boldsymbol{x}$ it is possible to compute the residuals

$$f_i = \frac{y_i - M(\boldsymbol{x}, u_i)}{\bar{y}},\ i = 1, \ldots, m, \tag{29}$$

where $\bar{y}$ is the average value of y. If a least squares fit is chosen, the parameters are determined as the minimizer $\boldsymbol{x}^{id}$ of the sum of the square residuals

$$F(\boldsymbol{x}) = \frac{1}{2} \sum_{i=1}^{m} (f_i(\boldsymbol{x}))^2. \tag{30}$$

The minimization strategy is specific to the optimization algorithm, which in the present case is a subspace trust region method and is based on the interior-reflective Newton method (Optimization Toolbox™ 4 User's Guide, 2008). A synthetic flowchart of the proposed identification algorithm is presented in figure 4. The input data consists of the experimental time-displacement curve which is interpolated on a grid of m equally-spaced points $(t_1, h_1), \ldots, (t_m, h_m)$ (in the present work m was set to 200). Each point (t_i, h_i) is assigned a weight $w_i \in [0, 1]$ to be multiplied by the respective residual f_i. Therefore the objective function (30) becomes

$$F(\boldsymbol{x}) = \frac{1}{2} \sum_{i=1}^{m} (w_i f_i(\boldsymbol{x}))^2. \tag{31}$$

Thus the influence on the final result of the less reliable portions of the curve, can be penalized (it is typically the case of the initial part of the ramp).

The vector $\boldsymbol{x}$ contains the poroelastic parameters to be identified. Although in the implemented routine, constant values can be assigned to known constitutive parameters, for the sake of generality, in the following it will be assumed that three constitutive parameters are to be identified. As it is the case for one dimensional consolidation (section 3), for indentation up to three constitutive parameters can be identified. Since κ and α, also in this case, only appear in the diffusivity coefficient (8) the seven possible sets of three parameters to be identified are:

1. (G, ν, κ)
2. (G, ν_u, κ)
3. (ν, ν_u, κ)
4. (G, ν, α)
5. (G, ν_u, α)

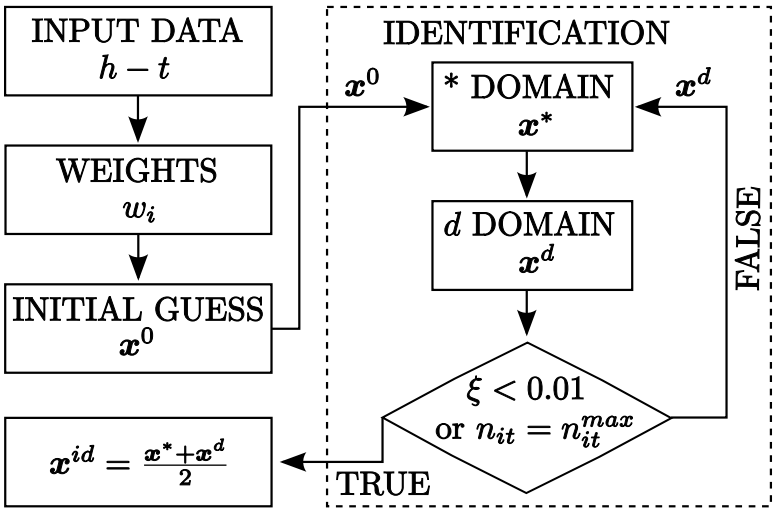

Figure 4: Flowchart of the identification algorithm featuring two optimization steps, one in the non-dimensional ($*$) domain, and the other in the dimensional (d) domain (see text for details).

6. (ν,ν_u,α)
7. (G,ν,ν_u)

In the following it will be assumed that the set of unknown parameters is (G,ν,κ). To start the identification process an initial guess of the parameter values (G^0, ν^0 and κ^0) has to be provided. Moreover these values are utilized to normalize the values of the parameters in the vector $\boldsymbol{x}$, which therefore is given by:

$$\boldsymbol{x}^T = \left(\frac{G}{G^0} \; \frac{\nu}{\nu^0} \; \frac{\kappa}{\kappa^0} \right). \tag{32}$$

This normalization improves matrix conditioning (Cugnoni et al., 2007). As is shown in figure 4, the core of the routine, the identification loop, consists of two nested optimizations, first in the normalized domain h^*t^*, then in the real ht domain. At each iteration both optimizations are carried out. In both cases a constrained optimization scheme is adopted and the objective functions are minimized in the parameter space defined by

$$\begin{aligned} G &\in \left(G^0 \cdot 10^{-2}, G^0 \cdot 10^2 \right), \\ \nu &\in (0, 0.45), \\ \kappa &\in \left(\kappa^0 \cdot 10^{-6}, \kappa^0 \cdot 10^6 \right). \end{aligned} \tag{33}$$

As it can be seen the bounds on G and κ are very loose, therefore the optimization with respect to these two parameters can be considered virtually unconstrained.

In the first optimization, for each input point (t_i, h_i) the corresponding (t_i^*, h_i^*) point is computed using the current values of the constitutive parameters $\boldsymbol{x}$. While the evaluation of t_i^* via (26) is straightforward, the evaluation of h_i^* requires assessing the values of $h_{\infty i}$ and h_{0i}, which were computed solving for h the 'corrected' Hertz's formula by Hay and Wolff (2001):

$$P = \eta \frac{4E}{3(1-\nu^2)} R^{\frac{1}{2}} h^{\frac{3}{2}}, \tag{34}$$

where the correction factor η is given by

$$\eta = 1 + \frac{2(1-2\nu)}{3\pi(1-\nu)} \sqrt{\frac{h}{R}}. \tag{35}$$

Note that for incompressible materials, as is the case for h_0 when the assumption $\nu_u = 0.5$ is made, (34) reduces to Hertz's formula ($\gamma = 1$). Using equation (34) is computationally more expensive than adopting Hertz's formula because there is no closed-form solution for h when $\nu \neq 0$, nevertheless it allows for better estimation of $h_{\infty i}$ and as a consequence more accurate values for h_i^*. This first optimization aims at finding the values of the constitutive parameters, gathered in the vector $\boldsymbol{x}^*$, which characterize the master curve from the database which best fits the normalized experimental points (t_i^*, h_i^*). The residuals are given by

$$f_i^* = \frac{h_i^* - h_{MCi}^*}{\overline{h^*}},\ i = 1, \ldots, m, \tag{36}$$

where h_{MCi}^* are the values assumed by the database master curve in correspondence of the values t_i^*.

In principle the identified parameter values $\boldsymbol{x}^*$ should already correspond to the best possible fit in the dimensional domain. Nevertheless what is done when normalizing the data according to (27) is essentially zooming in on the region of the displacement-time curve corresponding to the hold segment; as a consequence the procedure can be particularly sensitive to the noise in experimental data. In the second optimization stage it is checked that the results obtained in the normalized domain correspond to a good fit in the dimensional domain.

In the second optimization stage, the actual experimental points (t_i, h_i) are fit starting from the normalized experimental points (t_i^*, h_i^*) obtained at the end of the former optimization stage (the identified parameter values $\boldsymbol{x}^*$ are introduced as first parameter guess). The time-displacement curve $h^d(t)$ corresponding to $(t_1^*, h_1^*), \ldots, (t_m^*, h_m^*)$

is computed by solving (26) and (27) for t and h (again (34) is used to calculate $h_0^d(t)$ and $h_\infty^d(t)$). In this second optimization the residuals are given by

$$f_i^d = \frac{h_i - h_i^d}{\bar{h}},\ i = 1,\ldots,m, \tag{37}$$

where h_i^d are the values assumed by the curve $h^d(t)$ corresponding to the values t_i. Eventually this latter optimization stage provides a second set of constitutive parameters $\boldsymbol{x}^d$ to be introduced as new guess in the h^*t^* optimization stage.

To quantify the difference between the constitutive parameters in the two vectors $\boldsymbol{x}^*$ and $\boldsymbol{x}^d$ the norm ξ is defined

$$\xi = \sum_{i=1}^{3} \frac{\left|x_i^* - x_i^d\right|}{x_i^*}. \tag{38}$$

The identification loop is iterated until the difference between the constitutive parameters in the two vectors $\boldsymbol{x}^*$ and $\boldsymbol{x}^d$ is negligible. The convergence condition

$$\xi < 0.01 \tag{39}$$

is assumed. When (39) cannot be satisfied, the procedure is repeated until the maximum number of iterations $n_{it}^{max} = 50$ is reached. In this case the values of $\boldsymbol{x}^*$ and $\boldsymbol{x}^d$ which yield $min\,(\xi)$ are kept. The final output of the identification algorithm is the unique set of identified parameters $\boldsymbol{x}^{id}$ defined as the arithmetic average of $\boldsymbol{x}^*$ and $\boldsymbol{x}^d$:

$$\boldsymbol{x}^{id} = \frac{\boldsymbol{x}^* + \boldsymbol{x}^d}{2}. \tag{40}$$

6 Validation

The reliability of the proposed approach was ascertained by carrying out identification on $h(t)$ curves obtained by forward FE analyses. In particular the procedure was subjected to two tests:

- *Test 1*: Identification of poroelastic properties from five sets of FE-generated indentation displacement-time curves using randomly generated constitutive parameters;
- *Test 2*: Identification of constitutive parameters of three 'materials' having the same shear modulus and permeability but different Poisson's ratio, from data perturbed with $\pm 1\%$ white noise.

These identifications also allowed for quantification of the computing time requirements of the identification procedure. The maximum duration of one identification, which corresponds to the case of reaching the maximum number of iterations, on a personal computer equipped with a dual core 2.16 GHz cpu, was in the order of 1 minute. This result is particularly significant because it proves that the proposed approach allows for rapid analysis of large numbers of indentation tests.

Test 1

For the first test, five sets of values of constitutive properties were randomly chosen in the intervals

$$\begin{aligned} &G \in \left(G^r \cdot 10^{-1}, G^r \cdot 10^{1}\right), \\ &\nu \in (0, 0.45), \\ &\kappa \in \left(\kappa^r \cdot 10^{-2}, \kappa^r \cdot 10^{2}\right). \end{aligned} \tag{41}$$

where G^r and κ^r are reference values. To make the test more severe, the same criterion for the initial guess of parameters was adopted for all five sets as if the hypothetical user of the identification algorithm did not examine experimental curves before processing them for identification. The values of G^0 and ν^0 were estimated via Hertz's contact formula since for such an initial guess the application of the more complex formula by Hay and Wolff (34) does not lead to any improvement in the results. It was assumed that the indenter displacements at the end of the ramp and at the end of the test are $1.1h_0$ and $0.9h_\infty$ respectively, while κ^0 was assessed starting from the assumption that the rise time corresponds to $t^* = 1$ and solving (26) for κ. As previously discussed, the reliability of experimental (and FE) results for the ramp, and especially for its initial stages, is affected from the uncertainties to the onset and progress of contact and therefore the following strategy for the weights w_i was adopted:

$$\begin{aligned} &w_i = 0, \; t < 0.1t_R, \\ &w_i = \frac{t}{t_R} 0.1, \; t_R \leq t < t_R, \\ &w_i = 1, \; t \geq t_R. \end{aligned} \tag{42}$$

It can be seen that the first 10% of the ramp, when the specimen surface has just been engaged, is discarded while the following points have increasing influence on the indentation results as contact becomes well-established.

The properties assigned to the five 'materials' with randomly-generated poroelastic properties are summarized in table 1 along with the results of the identification. The identification of the shear modulus proves to be accurate: with the exception of

the fifth set of material properties, the obtained results for identified shear modulus G^{id} fall in the interval $G^{id}/G \pm 11\%$. Considering again sets 1 to 4, an analogous conclusion can be drawn for the permeability: the value of this parameter can span many orders of magnitude, therefore the fact that the maximum error in the identified values κ^{id} is about 40% can be considered a more than satisfactory result. The identification of Poisson's ratio proves to be more diffucult since it is particularly sensitive to the initial hypothesis on the values of h_0 and h_∞, as shown in equation (28): for sets 1 to 5 an average underestimation of about 30% is obtained. To understand the influence of the guess of the values of h_0 and h_∞ on the quality of the results, it is instructive to consider the identification relative to set 5. The results reported in table 1 are satisfactory but less accurate than those for set 1 to 4 with errors of 21%, 36% and 157% on G, ν and κ, respectively. Examination of the target curve $h(t)$ plotted in figure 5, it is clear that, towards the end of the test, the curve is almost flat; therefore the assumption that the indentation depth at the end of the test is 90% of the asymptotic value clearly leads to an overestimation of h_∞. A more appropriate hypothesis would be that at the displacement at end of the test corresponds to $0.98h_\infty$. The identified parameters corresponding to this latter guess are reported in table 1 (the set is labeled '5^a'): it can be seen how the quality of the results has significantly improved: the errors on G, ν and κ decrease to 3%, 8% and 29%, respectively. This confirms that with just a qualitative assessment of the slope of the $h-t$ curve at the end of the test, the initial guess on parameter values and therefore the eventual results of the identification can be significantly improved. The comparison between the $h(t)$ curves identified with the two hypothesis on h_∞ is reported in figure 5. The difference between the two fits is minimal with the only significant difference being that the second assumption on the value of h_∞ leads to a better fit of the first part of the *ht* curve for the hold segment. This plot also illustrates how small the time dependent displacement is when Poisson's ratio is larger than 0.4.

Test 2

For the second test, the indenter time-displacement curves for three materials having the same shear modulus G^r and permeability κ^r, and of increasing values Poisson's ratio, $\nu = 0.15, 0.25, 0.35$, were perturbed with $\pm 1\%$ white noise, a level of noise which exceeds that typically found in instrumented indentation testing. For all the three sets of data the initial guess on the parameter values was made adopting the same strategy used for the first test: the displacements at the end of the ramp and at the end of the test were assumed to be $1.1h_0$ and $0.9h_\infty$ respectively, κ^0 was derived from the assumption that the rise time corresponds to $t^* = 1$ and the weights defined in (42) were employed. Identification was carried out for both

the original unperturbed data and for the perturbed data. The results summarized in table 2 show that the loss of accuracy in the identified results caused by the introduction of noise is not significant. For sets 1 and 2 only the error on the permeability increases noticeably, staying however within an acceptable level (42%) for a parameter which, as already mentioned, can span over orders of magnitude. In the case of set 3 the results regarding the perturbed data are even better than those on the original data; on the one hand, this suggests that the initial guess for the parameter values is the primary factor in the final outcome of the identification, but on the other, this shows that the identification algorithm can tolerate the imposed level of noise even for the larger Poisson's ratio value. The plots of the original and perturbed data for set 1 with the respective identified curves and residuals are reported in figures 6 and 7. Both the fits in the *ht* domain and those in the h^*t^* domain are very good and the curves identified from the perturbed data exhibit the average trends in the residuals of the curves identified from the unperturbed data. Moreover in figure 7 it is possible to appreciate the amplification effect that the h^*t^* normalization has on the imposed noise.

Set	$\frac{G}{G^r}$	ν	$\frac{\kappa}{\kappa^r}$	$\frac{G^{id}}{G^r}$	ν^{id}	$\frac{\kappa^{id}}{\kappa^r}$	ξ	$\frac{G^{id}}{G}$	$\frac{\nu^{id}}{\nu}$	$\frac{\kappa^{id}}{\kappa}$
1	8.50	0.06	4.86E-01	8.08	0.06	2.82E-01	0.001	0.95	1.01	0.58
2	0.21	0.28	4.60E+01	0.23	0.16	4.77E+01	0.029	1.11	0.58	1.04
3	0.93	0.13	1.47E+01	0.94	0.07	1.05E+01	0.007	1.01	0.60	0.71
4	3.98	0.25	6.80E+01	4.25	0.15	6.39E+01	0.014	1.07	0.63	0.94
5	8.20	0.41	3.69E-02	9.94	0.26	9.49E-02	0.039	1.21	0.64	2.57
5^a	8.22	0.41	3.69E-02	8.43	0.38	2.62E-02	0.036	1.03	0.92	0.71

Table 1: Summary of the randomly generated constitutive parameters (G, ν and κ) for the five sets of data considered in Test 1 and corresponding identified results. The subscript r indicates the reference values with respect to which the parameters were normalized while the superscript *id* indicates the identified values. The results for set 5^a were obtained utilizing a different initial guess of the parameter values (see text for details). The value of the error norm ξ was computed according to (38).

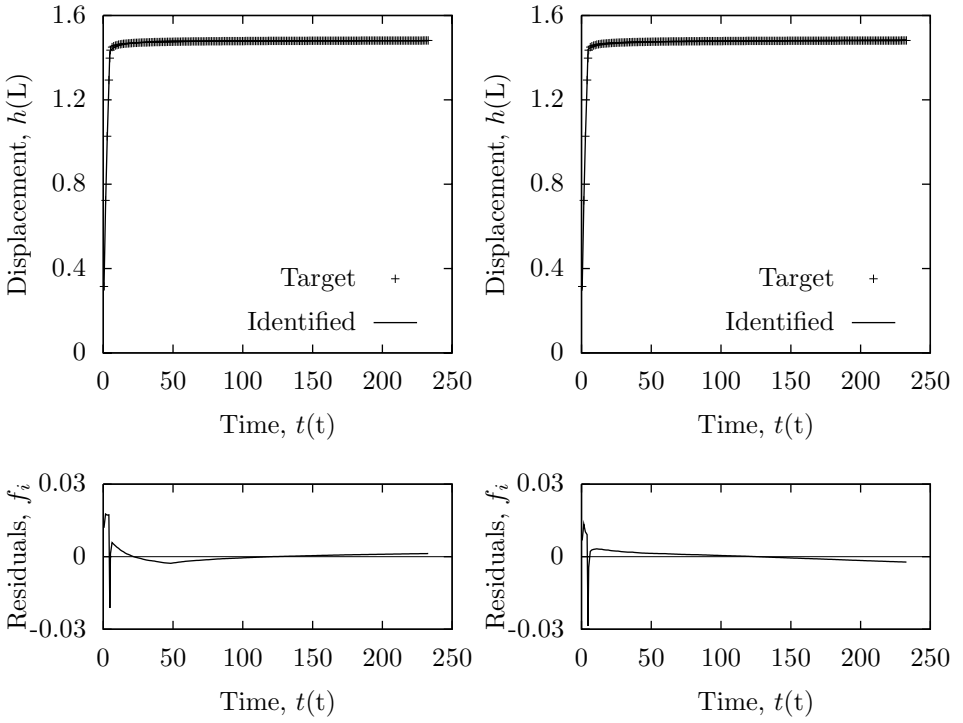

Figure 5: Results for validation test 1, identification of the fifth set (table 1) of randomly generated constitutive parameters (the units for t and h are time (t) and length (L), respectively). The identified $h(t)$ curve on the left and the respective residuals f_i are relative to the first guess on the value of h_∞ (the displacement at end of the test corresponds to $0.9h_\infty$); the identified $h(t)$ curve and the residuals f_i on the right are relative to the second guess on the value of h_∞ (the displacement at end of the test corresponds to $0.98h_\infty$). The difference between the two fits is minimal, but the second guess leads to a more accurate identification of the constitutive parameters.

7 Application Examples

The identification procedure was tested on experimental data from two extreme types of spherical indentation test: a 'macroindentation' test, 12.7 mm indenter radius, on gelatin gel and a nanoindentation test, 21 μm indenter radius, on bone immersed in water. This exercise was aimed at further benchmarking the algorithm rather than at an actual material characterization, therefore only one experimental curve for each material was considered, and the description of the specimen prepa-

		unperturbed data				perturbed data			
Set	ν	ξ	$\frac{G^{id}}{G^r}$	$\frac{\nu^{id}}{\nu}$	$\frac{\kappa^{id}}{\kappa^r}$	ξ	$\frac{G^{id}}{G^r}$	$\frac{\nu^{id}}{\nu}$	$\frac{\kappa^{id}}{\kappa^r}$
1	0.15	0.005	0.98	0.92	0.87	0.004	0.96	1.03	0.77
2	0.25	0.005	1.00	0.89	0.90	0.004	1.05	0.73	1.42
3	0.35	0.012	1.09	0.78	1.82	0.010	1.05	0.84	1.65

Table 2: Summary of the results of the identification of the parameters G, ν and κ for the three sets of data utilized in Test 2. The shear modulus and the permeability were assigned the reference values G^r and κ^r in all the three cases, while the value of Poisson's ratio increased from set 1 to 3. The superscript *id* indicates the identified values. The perturbed data were obtained by applying $\pm 1\%$ white noise to the unperturbed time-displacement curve (see text for details). The value of the error norm ξ was computed according to (38).

ration and testing is limited to few essential notes. Gelatin from porcine skin, 250 g Bloom, in powder form (Sigma-Aldrich Chemie GmbH, Steinheim, Germany) was dissolved in water, weight ratio gelatin to water 1:4, at 55°C, under moderate agitation for 15 minutes. The solution was then cast in a glass mold and kept at room temperature for 24 hours. A cylindrical specimen of about 40 mm height and 70 mm diameter was obtained. The indentation test was carried out on an Instron 5544 (Instron, High Wycombe, UK) testing apparatus equipped with a 5 N load cell. The maximum imposed load was 0.5 N, with a ramp of 20 s and a hold time of 180 s. The experimental data for bone was taken from a previous study on the mechanical response of bone immersed in different solvents (Bembey et al., 2006) and the median curve considered here is the same one analyzed by Oyen (2008). The maximum imposed load was 0.025 N, with a ramp of 25 s and a hold time of 120 s. The reader is referred to the cited article for a complete description of the experimental procedure .

As discussed early, up to three constitutive parameters can be identified from an indentation tests, therefore assumptions were made on the values of the remaining two. For both materials G, ν and κ were the identified parameters and the values of ν_u and α were imposed. For both materials it was assumed $\nu_u = 0.5$, and in the case of gelatin it was assumed that the constituents are incompressible, therefore $\alpha = 1$, while in the case of bone, the assumption $\alpha = 0.14$ was made (Cowin, 2004). As in the case of the tests used for the validation of the identification procedure, the initial guess of the parameter values, both for the gel and for bone, was derived

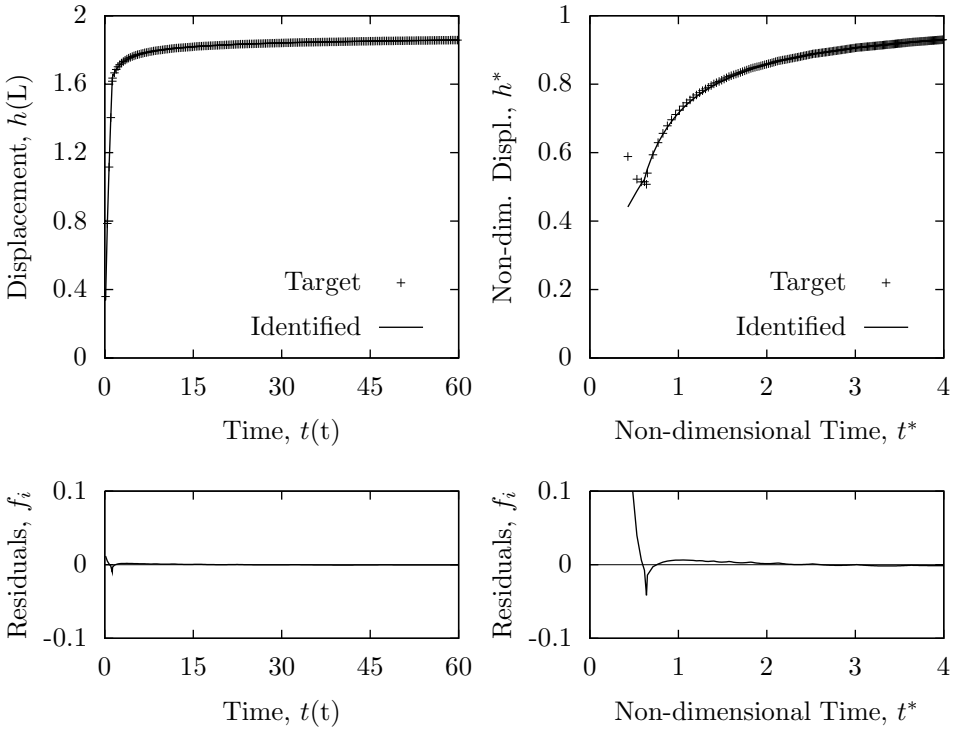

Figure 6: Results for validation test 2, identification of the first set (table 1) of randomly generated constitutive parameters without noise (the units for t and h are time (t) and length (L), respectively). Both the fit of the $h(t)$ curve and that of the $h^*(t^*)$ are satisfactory with only the first $h^*(t^*)$ point being off target, however its influence on the identification results is negligible as it is heavily penalized by the adopted weighting strategy (42)

from the assumption that the indenter displacements at the end of the ramp and at the end of the test are $1.1h_0$ and $0.9h_\infty$ respectively, while the rise time corresponds to $t^* = 1$. The identified values of G, ν and κ were $2.42{\cdot}10^{-2}$ MPa, 0.185, and 1.1 $\mathrm{mm^4N^{-1}s^{-1}}$ for gelatin and 466 MPa, 0.259, and $6.5{\cdot}10^{-8}$ $\mathrm{mm^4N^{-1}s^{-1}}$ for bone. To check the quality of the identification, forward FE simulations of the experiments were carried out, using as input data the identified properties. The features of the adopted FE models are in line with those of the models used to create the master curve database and are not reported for the sake of brevity. Comparisons between the experimental data, the obtained fit using the proposed identification procedure and the results of the forward FE simulations are reported in figure 8. It can be appreciated how there is complete agreement of the three sets of data in both

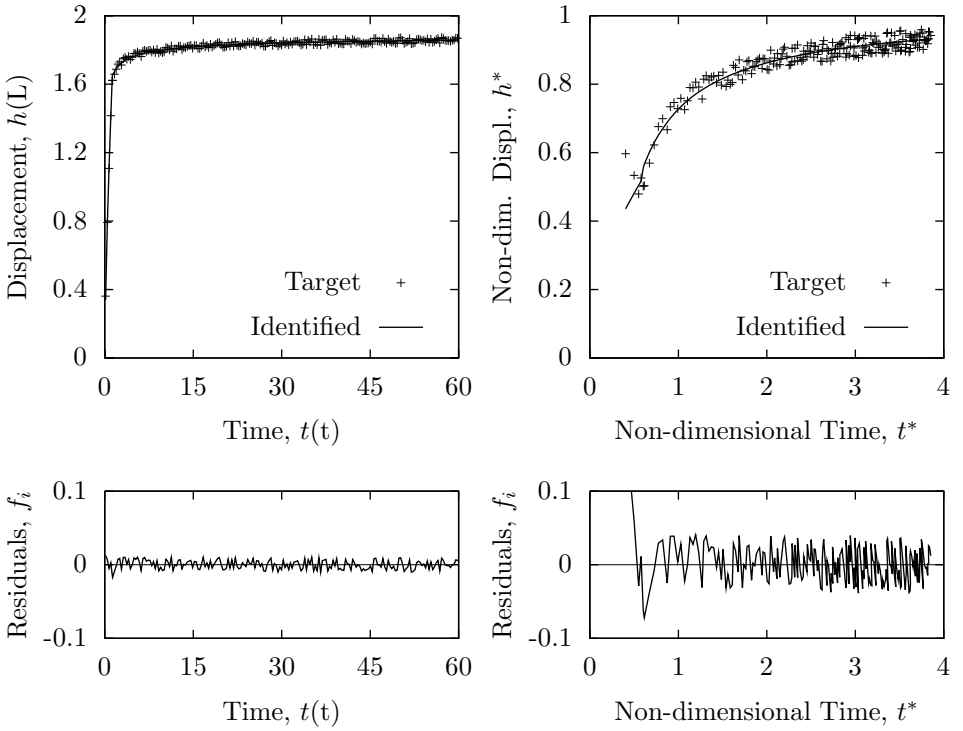

Figure 7: Results for validation test 2, identification of the first set (table 1) of randomly generated constitutive parameters with $\pm 1\%$ noise (the units for t and h are time (t) and length (L), respectively). Both the fit of the $h(t)$ curve and that of the $h^*(t^*)$ are satisfactory, exhibiting the average trend in the residuals of the curves identified from the unperturbed data (figure 6). The plots of the residuals show how the noise is significantly amplified by the normalization.

cases.

These two examples of the application of the identification approach highlight the intrinsic advantage the master-curve method has on other identification methods based on a database of dimensional solutions, e.g. Gupta et al. (2008): the same database of master curves can be applied to any kind of material, any ramp-hold profile and any indenter radius. The only caveat is that the deformation of the solid skeleton should not significantly exceed its elastic limit, since it is assumed that there are no material property alterations beneath the indenter. To have an estimate of the strain level in the material the formula $\varepsilon_R = 0.2\sqrt{h/R}$ (Johnson, 2003) can be employed, where ε_R is a representative strain, to be compared with the elastic

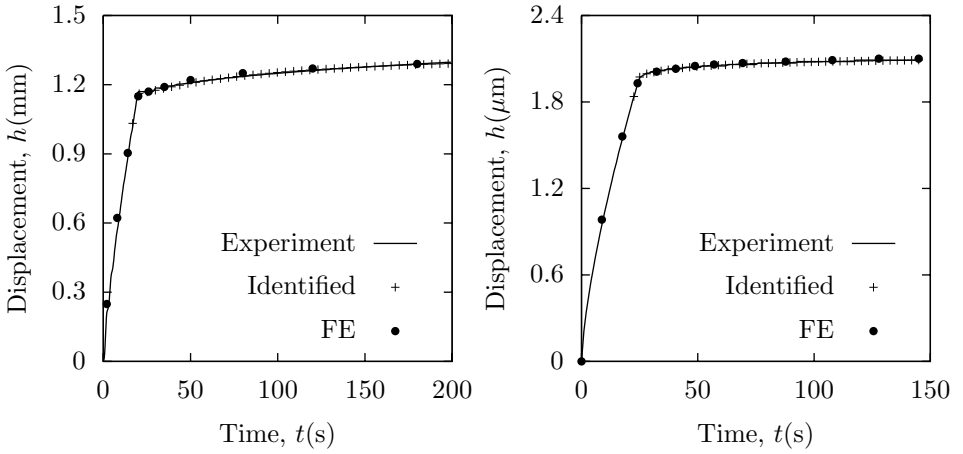

Figure 8: Application of the identification procedure to actual experimental data: 'macroindentation' of a gelatin gel (left) and nanoindentation of bone immersed in water (right). The applied loads are 0.5 N and 25 mN, respectively. In both cases the identification algorithm lead to a very good fit of experimental data. The quality of the identification is further demonstrated by the excellent agreement with the results of forward FE simulations, using the identified poroelastic parameters as input material properties.

strain limit.

8 Conclusions

A method for the identification of material poroelastic parameters from ramp-hold spherical indentation test is proposed. The procedure is based on a database of nondimensional master curves, therefore it is applicable to any pertinent experimental data independent of material properties, indenter radius and lengths of the ramp and hold segments. The approach proves to be effective in terms of both required computational effort and accuracy: the identification of three constitutive parameters, from one experimental curve, takes about one minute. Although the uniqueness of the solution cannot be assured, if a sensible guess of the initial parameters is introduced in the identification algorithm, the accuracy in the obtained results is good. Moreover such a guess can easily be drawn from a qualitative assessment of the time-displacement curve and, in particular, from an estimation of the value of the asymptotic displacement. Herein the application of the identification algorithm was limited to the case of $\nu_u = 0.5$ and to a permeable indenter, nevertheless the inclusion of a variable undrained Poisson's ratio and of the inden-

ter impermeability is straightforward as it would only require an enlargement of the master curve database.

Acknowledgement: The authors acknowledge Dr. J. Cugnoni for useful discussion. M. Galli was supported by Grant No. PBELB-120953 from the Swiss National Science Foundation.

References

Agbezuge, L.K.; Deresiewicz, H. (1974): On the Indentation of a Consolidating Half-Space. *Israel Journal of Technology*, vol. 12, pp. 322–338.

Bembey, A.K.; Oyen, M.L.; Bushby, A.J.; Boyde, A. (2006): Viscoelastic properties of bone as a function of hydration state determined by nanoindentation. *Philosophical Magazine*, vol. 86, no. 33–35, pp. 5691–5703.

Bucaille, J.L.; Stauss, S.; Felder, E.; Michler, J. (2003): Determination of Plastic Properties of Metals by Instrumented Indentation Using Different Sharp Indenters. *Acta Materialia*, vol. 51, no. 6, pp. 1663–1678.

Bucaille, J.L.; Rossoll, A.; Moser, B.; Stauss, S.; Michler, J. (2004): Determination of the Matrix In Situ Flow Stress of a Continuous Fibre Reinforced Metal Matrix Composite Using Instrumented Indentation. *Materials Science and Engineering A*, vol. 369, no. 1–2, pp. 82–92.

Chiarelli, P. (2004): The Poro-elastic Behavior of a Gel Thin Tube. *Materials Science and Engineering C*, vol. 24, pp. 463–47.

Constantinides, G.; Ravi Chandran, K.S.; Ulm, F.-J.; Van Vliet, K.J. (2008): Grid indentation analysis of composite microstructure and mechanics: Principles and validation. *Materials Science and Engineering A*, vol. 430, pp. 189–202

Coussy, O. (2004): *Poromechanics*, Wiley, Chichester, UK.

Cowin, S.C. (1999): Bone Poroelasticity. *Journal of Biomechanics*, vol. 32, pp. 217–238.

Cugnoni, J.; Botsis, J.; Sivasubramanian, V.; Janczak-Rusch, J. (2007): Experimental and Numerical Studies on Size and Constraining Effects in Lead-Free Solder Joints. *Fatigue & Fracture of Engineering Materials and Structures*, vol. 30, no. 5, pp. 387–399.

Cuy, J.L.; Mann,A.B; Livi, K.J.; Teaford, M.F.; Weihs, T.P. (2002): Nanoindentation Mapping of the Mechanical Properties of Human Molar Tooth Enamel. *Archives of Oral Biology*, vol. 47, pp. 281–291.

Deresiewicz, H. (1976): On the Indentation of a Consolidationg Half-Space II. Effect of Poisson's Ratio. *Israel Journal of Technology*, vol. 15, pp. 89–97.

Detournay, E.; Cheng, A.H.-D. (1993): Fundamentals of Poroelasticity. In: Fairhurst, C.; (Ed.), *Comprehensive Rock Engineering: Principles, Practice and Projects, Vol. II, Analysis and Design Method*, Pergamon, pp. 113–171.

Ebenstein, D.M.; Pruitt, L.A. (2006): Nanoindentation of Biological Materials. *Nanotoday*, vol. 1, no. 3, pp. 26–33.

Galli, M.; Cugnoni, J.; Botsis, J.; Janczak-Rusch, J. (2008): Identification of the Matrix Elastoplastic Properties in Reinforced Active Brazing Alloys. *Composites Part A*, vol. 39, pp. 972–978.

Galli, M.; Oyen, M.L. (2008): Spherical Indentation of a Finite Poroelastic Coating. *Applied Physics Letters*, vol. 93, 031911.

Galli, M.; Comley, K.S.C.; Shean, T.A.V.; Oyen, M.L. (2009): Viscoelastic and Poroelastic Mechanical Characterization of Hydrated Gels. *Journal of Materials Research*, vol. 24, no. 3, pp. 973–979.

Gupta, S.; Lin, J.; Ashby, P.; Pruitt, L. (2008): A fiber reinforced poroelastic model of nanoindentation of porcine costal cartilage: A combined experimental and finite element approach. *Journal of the Mechanical Behavior of Biomedical Materials*, doi:10.1016/j.jmbbm.2008.09.003

Hay, J.L.; Wolff, P.J. (2001): Small Correction Required when Applying the Hertzian Contact Model to Instrumented Indentation Data. *Journal of Materials Research*, vol. 16, no. 5, pp. 1280–1286.

Hsueh, C.-H.; Miranda, P. (2004): Master Curves for Hertzian Indentation on Coating/Substrate Systems. *Journal of Materials Research*, vol. 19, no. 1, pp. 94–100.

Huber, N.; Tsakamakis, C. (1999): Determination of Constitutive Properties from Spherical Indentation Data Using Neural Networks. Part I: the Case of Pure Kinematic Hardening in Plasticity Laws. *Journal of the Mechanics and Physics of Solids*, vol. 47, pp. 1569–1588.

Huber, N.; Tsakamakis, C. (1999): Determination of Constitutive Properties from Spherical Indentation Data Using Neural Networks. Part II: Plasticity with Nonlinear Isotropic and Kinematic Hardening. *Journal of the Mechanics and Physics of Solids*, vol. 47, pp. 1589–1607.

Huber, N.; Konstantinidis, A.; Tsakamakis, C. (2001): Determination of Poisson's Ratio by Spherical Indentation Using Neural Networks–Part I: Theory. *Journal of Applied Mechanics*, vol. 68, pp. 218–223.

Huber, N.; Konstantinidis, A.; Tsakamakis, C. (2001): Determination of Poisson's Ratio by Spherical Indentation Using Neural Networks–Part II: Identification Method. *Journal of Applied Mechanics*, vol. 68, pp. 224–229.

Hui, C.-Y.; Muralidharan, V. (2005): Gel Mechanics: a Comparison of the Theories of Biot and Tanaka, Hocker, and Benedek. *Journal of Chemical Physics*, vol. 123, 154905.

Hui, C.-Y.; Lin, Y.-Y.; Chuang, F.-C.; Shull, K.R.; Lin, W.-C. (2005): A Contact Mechanics Method for Characterizing the Elastic Properties and Permeability of Gels. *Journal of Polymer Science*, 43, pp. 359–370.

Johnson, K.L. (2003): *Contact Mechanics*. Cambridge University Press, Cambridge, UK.

Kochina, N.N. (1971): Changes in ground water level in irrigated terrain. *Journal of Applied Mechanics and Technical Physics*, vol. 12, no. 4, pp. 559–565.

Lin, Y.-Y.; Hu, B.-W. (2006): Load Relaxation of a flat rigid circular indenter on a gel half space. *Journal of Non-Crystalline Solids*, vol. 352, pp. 4034–4040.

Liu, K.; VanLandingham, M.R.; Ovaert, T.C. (2009): Mechanical characterization of soft viscoelastic gels via indentation and optimization-based inverse finite element analysis. *Journal of the Mechanical Behavior of Biomedical Materials*, doi:10.1016/j.jmbbm.2008.12.001.

Liu, D.S.; Tsai, C.Y. (2009): Estimation of thermo-elasto-plastic properties of thin-film mechanical properties using MD nanoindentation simulations and an inverse FEM/ANN computational scheme. *CMES: Computer Modeling in Engineering & Sciences*, vol. 39, no. 1, pp. 29–47.

McNamee, J.; Gibson, R.E. (1960): Displacement functions and linear transforms applied to diffusion through poroelastic media. *Quarterly Journal of Mechanics and Applied Mathematics*, vol. 13, pp. 98–111.

McNamee, J.; Gibson, R.E. (1960): Plane Strain and Axially Symmetric Problems of the Consolidation of a Semi-Infinte Clay Stratum. *Quarterly Journal of Mechanics and Applied Mathematics*, vol. 13, pp. 210–227.

Mesarovic, S.D.; Fleck, N.A. (1999): Spherical indentation of elastic-plastic solids. *Proceedings of the Royal Society A*, vol. 455, pp. 2707–2728

Olberding, J.E.; Suh J.K.F. (2006): A dual optimization method for the material parameter identification of a biphasic poroviscoelastic hydrogel: Potential application to hypercompliant soft tissues. *Journal of Biomechanics*, vol. 39, no. 13, pp. 2468–2475.

Olson, R.E. (1977): Consolidation under Time Dependent Loading. *Journal of the Geotechnical Engineering division, ASCE*, vol. 103, no. 1, pp. 55–60.

Oyen, M.L. (2008): Poroelastic Nanoindentation Responses of Hydrated Bone. *Journal of Materials Research*, vol. 23, pp. 1307–1314.

Schiffman, R.L. (1958): Soil Consolidation under Time-Dependent Loading. *Proceedings of Highway Research Board*, vol. 37, pp. 586–616.

Selvadurai, A.P.S.; Yue, Z.Q. (1994): On the Indentation of a Poroelastic Layer. *International Journal for Numerical and Analytical Methods in Geomechanics*, vol. 18, pp. 161–175.

Selvadurai, A.P.S. (2004): Stationary Damage Modelling of Poroelastic Contact. *International Journal of Solids and Structures*, vol. 41, pp. 2043–2064.

Selvadurai, A.P.S. (2007): The Analytical Method in Geomechanics. *Applied Mechanics Review*, vol. 60, pp. 87–106.

Simon, B.R. (1992): Multiphase Poroelastic Finite Element Models for Soft Tissue Structures. *Applied Mechanics Reviews*, vol. 45, pp. 191–218.

Terzaghi, K. (1923): Die Berechnung der DurchlÄssigkeit des Tones aus dem Verlauf der hydrodynamischen Spannungserscheinungen. *Sitzungsberichte Akademie der Wissenschaften, Wien Mathematisch- Naturwissenschaftliche Klasse, Abteilung IIa*, vol. 132, pp. 125–138.

The MathWorks Inc. (2008): *Optimization Toolbox™4 User's Guide*.

Wang, H.F. (2000): *Theory of Linear Poroelasticity with Applications to Geomechanics and Hydrogeology*. Princeton University Press, Princeton, NJ, USA.

Warner, M.D.; Taylor, W.R.; Clift, S.E. (2001): A Method for Automatically Determining Contact between a Non-Porous Surface and Articular Cartilage in a Biphasic FE Model. *Computer Methods in Biomechanics and Biomedical Engineering*, vol. 4, pp. 207–212.